Modeling for bipolar resistive memory switching in transition-metal oxides

Ji Hyun Hur, Myoung-Jae Lee,* Chang Bum Lee, Young-Bae Kim, and Chang-Jung Kim
Semiconductor Laboratory, Samsung Advanced Institute of Technology, Gyeonggi-Do 446-712, Korea
(Received 11 August 2010; revised manuscript received 1 October 2010; published 25 October 2010)

A model which describes the bipolar resistive switching in transition-metal oxides is presented. To simulate the effect of switching, we modeled results of doping by oxygen vacancies along with variable Schottky barrier and resistor. The model simultaneously predicts three key features of experimental measurements: the rectifying behavior in high resistance states, abrupt switching, and the existence of bistable resistance states. Our model is based on modulation of Schottky barrier formed by variable resistance oxide layer at the metal-oxide interface. Experimental measurements of the $Pt/Ta_2O_5/TaO_x/Pt$ structure matched very well with our nonvolatile resistive switching model.

DOI: 10.1103/PhysRevB.82.155321 PACS number(s): 71.30.+h, 71.55.Ht, 72.10.Bg

I. INTRODUCTION

As a successor to charge-based memories such as flash memories, resistance-based memories have been the focus of attention. Contrary to charge storage, resistance-based memories rely on voltage induced mechanisms such as nanofilament formation,[1] phase change,[2] ionic bridge formation,[3] Schottky barrier or domain modulation,[4,5] and metal-insulator transition.[6] Each of these mechanisms has been shown to scale down well to sizes beyond the flash scaling limitation making resistance-based memories a promising candidate for future nonvolatile memory applications. There still exist limitations mostly related to high current-density issues or reliability in implementing next-generation memories into product lines.[7]

Resistance random access memory (ReRAM) refers to usually oxide-based materials which show reversible resistance changes through either filament formation such as NiO (Refs. 1 and 8) or Schottky barrier modulation such as in the case of perovskite materials[4,9–11] and TaO_x.[12] Depending on materials, device structures and operational conditions, thin oxide semiconductor layer at the electrode interface can act as a tunneling layer or Schottky barrier.[13] While lots of experimental results for Schottky barrier involved bipolar ReRAM switching have long been given, a clear explanation of the switching process has never been proven. The lack of a successful model in predicting ReRAM switching has led to trial and error as the experimental method of improving ReRAM performance.

In this work, we report a physical model to explain bipolar oxide ReRAM switching based on the interface Schottky barrier modulation caused by thin oxide-layer doping-level variation. The oxide semiconductor layer resistance is could be changed by electric field driven oxygen-vacancy doping[14–17] resulting in Schottky barrier modulation at the same time.

II. THEORETICAL MODEL

We show that this can excellently explain ReRAM memory switching behavior both qualitatively and quantitatively. Furthermore the three key aspects of experimental measurements are described with our model: the rectifying behavior,[18] abrupt switching, and bistable resistance states.

Figure 1 demonstrates the overall physical system used to model the system. In Fig. 1(a), the $Pt/Ta_2O_5/TaO_x/Pt$ structure is shown with positively charged oxygen vacancies in the nonstoichiometric TaO_x layer. Previous reports[12] have reported a correlation between oxygen vacancies and resistive switching and therefore they are represented. Meanwhile Fig. 1(b) shows a conducting path of the low resistance state (LRS) which forms within the Ta_2O_5 layer after forming. The forming process[18] involves applying a negative bias on the top electrode of 2–3 V for 4-nm-thick Ta_2O_5 and 20 nm

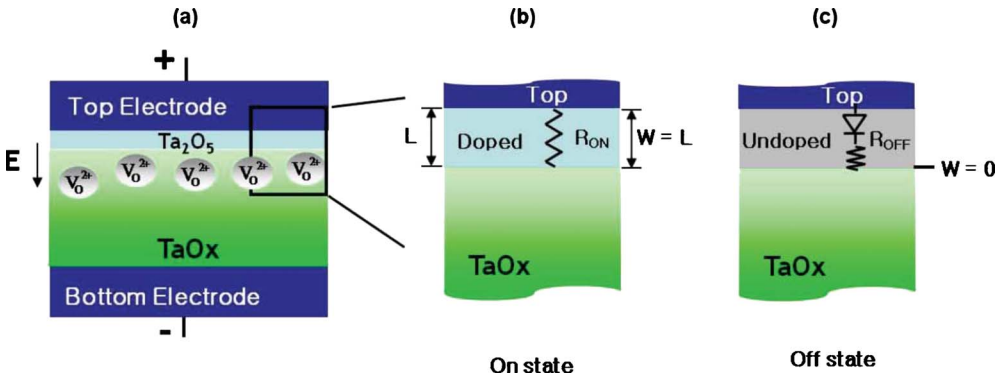

FIG. 1. (Color online) Conceptual schematic of bipolar resistance switching. (a) Overall schematic. (b) On-state assumption, $W=L$ doped region in ohmic state. (c) Off-state assumption, no doped layer $W=0$ with Schottky barrier in the top interface.

TaO_x base layers. Forming is believed to create the conducting path required for switching[1,12] while subsequent switching is focused in more local regions of conducting path in Ta_2O_5 layer rather than involving the entire Ta_2O_5/TaO_x layer.[12] Further evidence of this model is given by our experimental measurements. Oxygen-vacancy transport in conducting path is determined by following equation of motion:[14]

$$\frac{dw(t)}{dt} = \mu_V \frac{R_{ON}}{L^3} i(t) w(t)[L - w(t)]. \tag{1}$$

Here, $w(t)$, μ_V, R_{ON}, and $i(t)$ are oxygen-vacancy-doped region length, oxygen-vacancy mobility, resistance, current of fully doped state ($w=L$), respectively. Meanwhile L is defined as active oxide thickness as shown in Figs. 1(b) and 1(c). Externally applied voltage $V(t)$ can be expressed in terms of model variables as follows:

$$V(t) = \left\{ R_{ON} \frac{w(t)}{L} + R_{OFF}\left[1 - \frac{w(t)}{L}\right] + R_0 \right\} i(t) \equiv R(t) i(t), \tag{2}$$

where R_{OFF} is resistance for fully undoped state ($w=0$) and R_0 is TaO_x base layer resistance. Combining Eqs. (1) and (2), we can obtain first-order differential equation of $w(t)$ in terms of applied voltage $V(t)$ as

$$\frac{dw(t)}{dt} = \frac{\mu_V R_{ON} w(t)[L - w(t)] V(t)}{L^3 \{R_{ON} w(t)/L + R_{OFF}[1 - w(t)/L] + R_0\}}. \tag{3}$$

After forming, the voltage-current response of TaO_x memory device shows ohmic behavior[8] therefore we can safely assume that on state which means the entire conducting path region is doped with oxygen vacancies, has ohmic contact with electrodes.

A reset operation to return the device to the high resistance state (HRS) is shown in Fig. 1(c). The interface of the conducting path will return to the insulating state by oxidation[1] and form a Schottky contact of which barrier height is determined by the difference between Pt work function[19] and the effective electron affinity of TaO_x thin film.[20] Bistable switching occurs as the conducting path is oxidized or reduced at the metal electrode-oxide layer interface.[1]

Then the system can be described by electric conduction through Schottky barrier which is serially connected with variable resistance $R(t)$,[21]

$$I(t) = \begin{cases} I_0 \left[\exp\left\{ \dfrac{q}{\eta k T}[V(t) - I(t)R(t)] \right\} - 1 \right] & \text{for } V > 0 \\ I_0 & \text{for } V < 0, \end{cases} \tag{4}$$

$$I_0 = A A^* T^2 \exp(-q\phi_B / kT), \tag{5}$$

where A is electrode area, A^* is the Richardson constant, T is temperature which we took in all cases to be 300 K, ϕ_B is the effective Schottky barrier height, V is the applied bias, q is the electron charge, and k is the Boltzmann constant. The ideality factor eta (η) is given by[21]

$$\eta = 1 + \left(\frac{\delta}{\varepsilon_i}\right) \frac{(\varepsilon_s / W_D) + q D_{its}}{1 + (\delta/\varepsilon_i) q D_{itm}}, \tag{6}$$

where δ is the metal-semiconductor interfacial layer thickness, ε_i is the dielectric constant of the insulator, ε_s is the dielectric constant of the semiconductor, W_D is the depletion layer thickness, D_{its} and D_{itm} are the interfacial trap densities in the semiconductor and insulator, respectively. Taking into account that the trap sites are originated from oxygen vacancies,[22,23] and assuming that interfacial trap densities are same for both sides at off state,

$$\eta \cong 1 + \frac{D_{its}}{D_{itm}} \cong \begin{cases} 2 & \text{at off state} \\ \gg 1 & \text{at on state.} \end{cases} \tag{7}$$

As oxygen vacancies are doped in conduction path, the trap density in oxide semiconductor is also increased. We take the on-state trap density as 50 times larger than that of off state. As we can see from the simulation results match closely to experimental ones when the η factor in Eq. (7) is about 50 times higher in the on state. Moreover the on/off ratio could be changed by adjusting the ideality factor, and in the on state, the symmetric *I-V* behavior changes to an asymmetric one. When all the conduction path is doped with oxygen vacancies, i.e., $w(t)=L$, Eq. (2) approaches ohm's law.

Effective Schottky barrier height ϕ_B for arbitrary voltage is expressed with electric field induced barrier lowering effect,

$$\phi_B = \phi_{B0} - \Delta\phi_B, \tag{8}$$

barrier lowering term $\Delta\phi_B$ is described by

$$\Delta\phi_B = \sqrt{\frac{qE_m}{4\pi\varepsilon}}, \tag{9}$$

where E_m is maximum electric field between electrode and oxide layer which can be expressed as

$$E_m = \frac{1}{\varepsilon_s}[n_s W_d + n_d w(t)], \tag{10}$$

where n_s, n_d, and W_d are base layer charge density, doped region charge density, and base-layer depletion width, respectively. Because doped region charge density is much larger than that of base layer, we can assume that $n_s W_d \ll n_d w(t)$ for $w(t) \neq 0$.

Considering oxide barrier height is proportional to square root of oxide thickness and assuming barrier height is vanished when $w(t)=L$, we can approximate ϕ_{B0} as

$$\phi_{B0} \approx \phi_{B0}\left(1 - \sqrt{\frac{w(t)}{L}}\right). \tag{11}$$

Here, the most important thing for the equation is that the ϕ_{B0} is varied for a $w(t)$ and near fully undoped state $[w(t) \sim 0]$, barrier height can be written in terms of detailed expression of W_D by

$$\phi_B \approx \phi_{B0} - \left(\frac{q^3 n_s \phi_{B0}}{8\pi^2 \varepsilon_s^3}\right)^{1/4} \left(1 - \frac{V}{4\phi_{B0}}\right). \tag{12}$$

From Eq. (4), negative voltage current for off state is

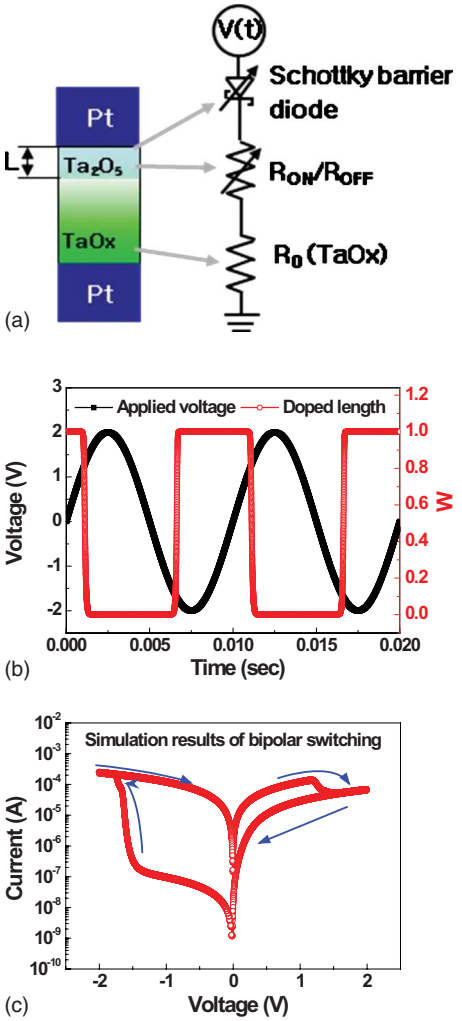

FIG. 2. (Color online) (a) Circuit Model with variable Schottky barrier, variable resistor, and base-layer resistance. (b) Sin wave voltage signal and response of doped region. (c) Results of bipolar resistance switching simulation.

$$I_{OFF}(V<0) = I_0\left\{1 - \frac{q}{4\phi_{B0}kT}\left(\frac{q^3 n_s \phi_{B0}}{8\pi^2\varepsilon_s^3}\right)^{1/4}[V - I_{OFF}R(t)]\right\}$$
$$\approx I_0[V - I_{OFF}R(t)], \quad (13)$$

therefore,

$$I_{OFF}(V<0) = \frac{I_0 V}{1 + I_0 R(t)}. \quad (14)$$

Figure 2(a) shows the equivalent circuit used in our model along with the structure of the cell that corresponds to each element. The voltage signal used in our model was a simple sinusoidal wave with amplitude 2 V and period 0.01 s as shown by closed black squares in Fig. 2(b). The open red circles show $w(t)$ variation following the voltage signal.

Using the voltage signal and η parameters in Eq. (4), we can reproduce the current-voltage behavior as shown in Fig. 2(c). The prefactor of A^*T^2 (unit: A m^{-2}) was estimated to be 1×10^{12} at 300 K, ϕ_{B0} is set to 0.6 eV, and the electrode area was 9×10^{-6} cm^2. As we can see, two features are immediately apparent. First is the rectifying behavior for the HRS. The rectifying comes from the fact that the conduction in HRS is governed by Schottky barrier electrical conduction mechanism. Next the abrupt switching from HRS to LRS and from LRS to HRS is modeled well by the change in volume of oxygen-vacancy-doped region and corresponding variation in ϕ_B, and bistable resistance states change is caused by two different oxygen-vacancy distributions, i.e., fully doped and fully undoped states.

III. COMPARISON TO EXPERIMENTAL DATA

In order to compare our model with experimental results, we fabricated a Pt/Ta_2O_5/TaO_x/Pt structure devices. First Pt bottom electrodes were deposited by rf magnetron sputtering, and then reactive rf magnetron sputtering was used to deposit a 45 nm TaO_x layer at 3% oxygen partial pressure, and substrate temperature of 400 °C. The sample was then plasma annealed at 500 °C by placing the sample in a chamber with argon and 10% oxygen plasma to form the Ta_2O_5 layer of ~4 nm. Finally the top Pt electrode layer was deposited by rf magnetron sputtering and cells were defined as 30 μm × 30 μm size using standard photolithography and lift off method.

A separate Pt/TaO_x/Pt sample fabricated without plasma annealing, showed resistivity values of $\sim2\times10^4$ Ω cm. Meanwhile the samples with plasma-annealed Ta_2O_5 layers $\sim2\times10^6$ Ω cm. Figures 3(a) and 3(b) show the Pt/TaO_x/Pt and Pt/Ta_2O_5/TaO_x/Pt transmission electron microscopy (TEM) images which show the clear formation of the Ta_2O_5 layer and x-ray photoelectron spectroscopy (XPS) images taken at varying Ar^+-ion sputtering times, respectively. The XPS depth profiles also indicate the formation of the Ta_2O_5 layer for plasma annealed samples through the two peaks Ta $4f_{7/2}$ at 26.2 eV and Ta $4f_{5/2}$ at 28.1 eV corresponding to Ta^{+5} binding energy which occurs in Fig. 3(b) but not in Fig. 3(a). This means that the stoichiometric Ta_2O_5 layer is well formed on the TaO_x layer by plasma oxidation.

Figure 3(c) is the current-voltage measurements of the two samples, the closed black squares show results from the Pt/TaO_x/Pt sample while the open red circles show the Pt/Ta_2O_5/TaO_x/Pt sample. The two bistable resistance states for the Pt/Ta_2O_5/TaO_x/Pt sample are shown to have resistance of 3.5–21.6 MΩ for the HRS and ~18 KΩ for the LRS at −5 V. The LRS resistance value for the Pt/Ta_2O_5/TaO_x/Pt sample corresponds well with the resistance of Pt/TaO_x/Pt sample fabricated without plasma annealing. Also, the HRS resistance value corresponds to the resistance of the Ta_2O_5 layer. Therefore, we conclude that resistance switching is likely to occur at the Pt/Ta_2O_5 interface through the connecting or disconnecting of a conducting path.

Meanwhile abrupt switching occurs at from high to low at ~−1.2 V and from low to high at ~2 V. The data shows 50 switching cycles for the Pt/Ta_2O_5/TaO_x/Pt sample.

Comparing the results from the modeling and actual experimental data, the exact same behavior can be observed. The parameters chosen closely model the differences in the high and low resistance states of three orders of magnitude

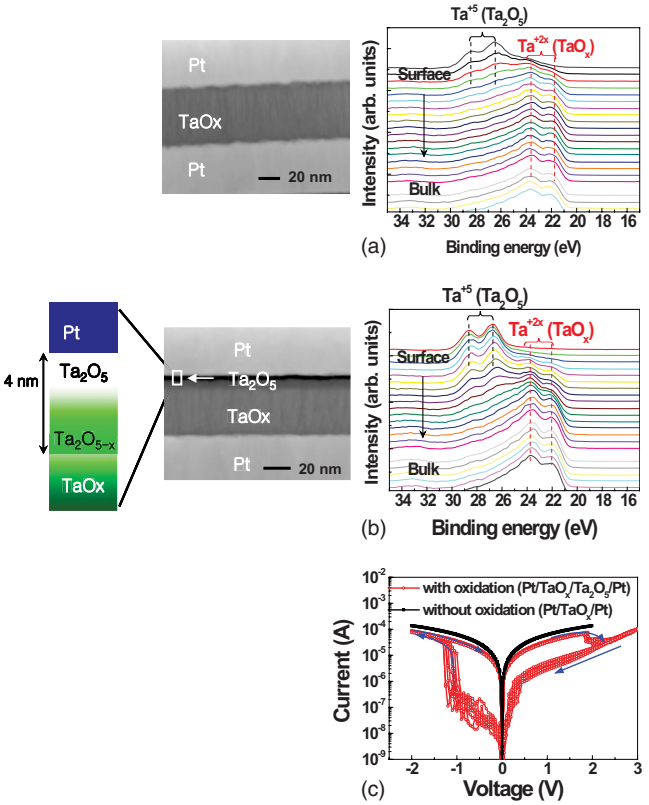

FIG. 3. (Color online) (a) TEM image and XPS depth profile of $Pt/TaO_x/Pt$ film. (b) TEM image and XPS depth profile of $Pt/Ta_2O_5/TaO_x/Pt$ film. (c) Experimental results from $Pt/TaO_x/Pt$ (black) and $Pt/Ta_2O_5/TaO_x/Pt$ (arrow) films.

for reverse bias and one order of magnitude for forward bias. The abrupt change to resistance past a certain threshold voltage is also clearly seen in both our model and the experimental data. Finally the rectifying characteristic which is more pronounced in the HRS is clearly predicted by the Schottky barrier model as well. Also, we have tested endurance of

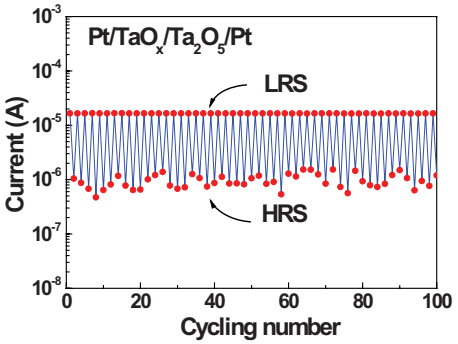

FIG. 4. (Color online) Endurance characteristics of $Pt/TaO_x/Ta_2O_5/Pt$ device. We used a −3 V pulse with 1 μs duration to switch from HRS to LRS, and a +3 V pulse with 1 μs duration to switch from LRS to HRS.

cells which is an important measurement for nonvolatile memory applications. Figure 4 shows 30 $\mu m \times 30$ μm size cells cycling 100 times. As compared to Fig. 3(c), there is little variance in the on-state resistance, and the off-state resistance variance is large. This is much like the resistance switching mechanism described in the simulation model which assumes that the trap density at the interface is different during each cycle. However, the endurance data show an average on/off ratio of slightly over one order of magnitude.

IV. SUMMARY

In summary, we have proposed a bipolar resistive switching model for a transition-metal oxide layer. By correlating Schottky barrier characteristics, i.e., ideality factor and barrier height with oxide-layer resistance state, several key aspects of the experimental data are well predicted. In future works, we hope to do a complete measurement of temperature dependence on switching to further verify the validity of our model.

*myoungjae.lee@samsung.com

[1] M.-J. Lee, S. Han, S. H. Jeon, B. H. Park, B. S. Kang, S.-E. Ahn, K. H. Kim, C. B. Lee, C. J. Kim, I.-K. Yoo, D. H. Seo, X.-S. Li, J.-B. Park, J.-H. Lee, and Y. Park, Nano Lett. **9**, 1476 (2009).

[2] D. Adler, M. S. Shur, M. Silver, and S. R. Ovshinsky, J. Appl. Phys. **51**, 3289 (1980).

[3] S. Dietrich, M. Angerbauer, M. Ivanov, D. Gogl, H. Hoenigschmid, M. Kund, C. Liaw, M. Markert, R. Symanczyk, L. Altimime, S. Bournat, and G. Mueller, IEEE J. Solid-State Circuits **42**, 839 (2007).

[4] A. Sawa, T. Fujii, M. Kawasaki, and Y. Tokura, Appl. Phys. Lett. **85**, 4073 (2004).

[5] M. J. Rozenberg, I. H. Inoue, and M. J. Sánchez, Phys. Rev. Lett. **92**, 178302 (2004).

[6] M. J. Rozenberg, I. H. Inoue, and M. J. Sánchez, Appl. Phys. Lett. **88**, 033510 (2006).

[7] M. J. Lee, S. I. Kim, C. B. Lee, H. Yin, S.-E. Ahn, B. S. Kang, K. H. Kim, J. C. Park, C. J. Kim, I. Song, S. W. Kim, G. Stefanovich, J. H. Lee, S. J. Chung, Y. H. Kim, and Y. Park, Adv. Funct. Mater. **19**, 1587 (2009).

[8] H. Shima, T. Nakano, and H. Akinaga, Appl. Phys. Lett. **91**, 012901 (2007).

[9] S. Tsui, A. Baikalov, J. Cmaidalka, Y. Y. Sun, Y. Q. Wang, Y. Y. Xue, C. W. Chu, L. Chen, and A. J. Jacobson, Appl. Phys. Lett. **85**, 317 (2004).

[10] A. Beck, J. G. Bednorz, Ch. Gerber, C. Rossel, and D. Widmer, Appl. Phys. Lett. **77**, 139 (2000).

[11] S. Q. Liu, N. J. Wu, and A. Ignatiev, Appl. Phys. Lett. **76**, 2749 (2000).

[12] Z. Wei, Y. Kanzawa, K. Arita, Y. Katoh, K. Kawai, S. Muraoka, S. Mitani, S. Fujii, K. Katayama, M. Iijima, T. Mikawa, T. Ninomiya, R. Miyanaga, Y. Kawashima, K. Tsuji, A. Himeno, T. Okada, R. Azuma, K. Shimakawa, H. Sugaya, T. Takagi, R. Yasuhara, K. Horiba, H. Kumigashira, and M. Oshima, IEEE

Int. Electron Devices Meet. Tech. Dig., 293 (2008).
[13] M. W. Allen and S. M. Durbin, Appl. Phys. Lett. **92**, 122110 (2008).
[14] D. B. Strukov, G. S. Snider, D. R. Stewart, and R. S. Williams, Nature (London) **453**, 80 (2008).
[15] J. J. Yang, M. D. Pickett, X. Li, D. A. A. Ohlberg, D. Stewart, and R. S. Williams, Nat. Nanotechnol. **3**, 429 (2008).
[16] G. Y. Yang, G. D. Lian, E. C. Dickey, and C. A. Randall, J. Appl. Phys. **96**, 7500 (2004).
[17] Y. B. Nian, J. Strozier, N. J. Wu, X. Chen, and A. Ignatiev, Phys. Rev. Lett. **98**, 146403 (2007).
[18] D. Lee, D.-J. Seong, I. Jo, F. Xiang, R. Dong, S. Oh, and H. Hwang, Appl. Phys. Lett. **90**, 122104 (2007).
[19] S. J. Tans, R. M. Verschuerenm, and C. Dekker, Nature (London) **393**, 49 (1998).
[20] Y. C. Yeo, Q. Lu, W. C. Lee, T.-J. King, C. Hu, X. Wang, X. Guo, and T. P. Ma, IEEE Electron Device Lett. **21**, 540 (2000).
[21] S. M. Sze and K. K. Ng, *Physics of Semiconductor Devices*, 3rd ed. (Wiley, New York, 2007), Sec. 3.3.6.
[22] H. Sawada and K. Kawakami, J. Appl. Phys. **86**, 956 (1999).
[23] R. Ramprasad, J. Appl. Phys. **94**, 5609 (2003).